Comparing microsphere deposition and flow modeling in 3D vascular trees

M. Marxen, J. G. Sled, L. X. Yu, C. Paget and R. M. Henkelman

Am J Physiol Heart Circ Physiol 291:2136-2141, 2006. First published Jun 9, 2006;
doi:10.1152/ajpheart.00146.2006

Am J Physiol Heart Circ Physiol 291: H2136–H2141, 2006.
First published June 9, 2006; doi:10.1152/ajpheart.00146.2006.

Comparing microsphere deposition and flow modeling in 3D vascular trees

M. Marxen,[1,2] J. G. Sled,[1,3] L. X. Yu,[3] C. Paget,[2] and R. M. Henkelman[1,2,3]

[1]*Department of Medical Biophysics, University of Toronto;* [2]*Sunnybrook and Women's College Health Sciences Centre, University of Toronto; and* [3]*Hospital for Sick Children Mouse Imaging Centre, Toronto, Ontario, Canada*

Submitted 8 February 2006; accepted in final form 3 June 2006

Marxen, M., J. G. Sled, L. X. Yu, C. Paget, and R. M. Henkelman. Comparing microsphere deposition and flow modeling in 3D vascular trees. *Am J Physiol Heart Circ Physiol* 291: H2136–H2141, 2006. First published June 9, 2006; doi:10.1152/ajpheart.00146.2006.—Blood perfusion in organs has been shown to be heterogeneous in a number of cases. At the same time, a number of models of vascular structure and flow have been proposed that also generate heterogeneous perfusion. Although a relationship between local perfusion and vascular structure has to exist, no model has yet been validated as an accurate description of this relationship. A study of perfusion and three-dimensional (3D) arterial structure in individual rat kidneys is presented, which allows comparison between local measurements of perfusion and model-based predictions. High-resolution computed tomography is used to obtain images of both deposited microspheres and of an arterial cast in the same organ. Microsphere deposition is used as an estimate of local perfusion. A 3D cylindrical pipe model of the arterial tree is generated based on an image of the arterial cast. Results of a flow model are compared with local microsphere deposition. High correlation ($r^2 > 0.94$) was observed between measured and modeled flows through the vascular tree segments. However, the relative dispersion of the microsphere perfusion measurement was two- to threefold higher than perfusion heterogeneity calculated in the flow model. Also, there was no correlation in the residual deviations between the methods. This study illustrates the importance of comparing models of local perfusion with in vivo measurements of perfusion in the same biologically realistic vascular tree.

perfusion heterogeneity; three-dimensional imaging; microcomputed tomography; casting; rat kidney; blood flow

PERFUSION IS DEFINED AS the volume of blood delivered to a certain mass or volume of tissue per unit time. With the use of microsphere deposition techniques (2, 11, 26) and imaging methods such as positron emission tomography (16), single photon emission computed tomography (22), magnetic resonance imaging (4), and computed tomography (CT; see Ref. 13), perfusion has been observed to be heterogeneous in a number of organs such as lungs (11), heart (2, 3, 14), muscle (14, 16), and kidneys (13). The heterogeneity is often presented by plotting the relative dispersion (RD = SD/mean) of perfusion as a function of sample mass. In many cases, these curves are found to resemble a power law relationship as a function of sample mass.

The local distribution of blood flow has to be reflected in the resistance distribution of the delivering vascular network. Many models of blood flow have been proposed that make predictions about the spatial distribution of perfusion (5, 12, 17, 18, 24, 29, 30). Although RD curves with similar power law parameters could be produced, none of these models have been validated by direct comparison with measurements of local perfusion in individual organs. This is due primarily to the fact that most models only match certain statistical features of realistic biological vascular trees and do not represent a particular organ. It is, therefore, a challenging task to establish a direct correspondence between local perfusion distributions in models and in real organs.

In this article, we present measurements of local perfusion in rat kidneys based on high-resolution computed tomography (microCT) images of microsphere deposition. At the same time, detailed pipe models of the arterial trees were generated from a second set of microCT images of arterial vascular casts in the same kidneys. A model of blood flow through the reconstructed model tree is calculated and is then compared with the experimental measurements.

MATERIALS AND METHODS

Experimental procedure and CT scanning. The animal procedure was approved by the animal care committee of Sunnybrook and Women's College Health Sciences Center. Several Wistar rats were anesthetized using ketamine-xylazine (75:10 mg/kg im) and maintained using halothane inhalant. This decreases the renal blood flow by 18% (8) but does not affect the conclusions of the study. The abdomen was opened, and the abdominal aorta was cannulated distally to the renal arteries. The heart was exposed through a midsternal incision, and ~4 ml of silver- and/or gold-coated, 17-μm-diameter, X-ray opaque microspheres (~10^6 particles, Ag/AuVIII-L1080; Microparticles, Berlin, Germany) suspended in Ringer solution were injected in the left atrium in ~10 s. After ~2 min of continued heart beating, the vascular system was flushed with heparinized Ringer solution through the catheter in the abdominal aorta. The blood was drained through a cut in the abdominal vena cava. Next, the thoracic aorta was clamped off with a hemostat, and perfusion was continued with Batson's no. 17 (5 ml of monomer, 1.5 ml catalyst, 100 μl of promoter, and a small amount of blue pigment; Polysciences, Warrington, PA). The viscosity of the casting agent and the perfusion pressure of ~80 mmHg was chosen such that only arterial vessels were filled with the resin. After ~2 h, the kidneys were excised and fixed in 30% ethanol for ~48 h. For CT scanning, the renal arteries were glued to an acrylic base, and the two kidneys were placed in separate cylindrical sample vials (28 mm diameter). The vials were filled with 30% ethanol, and CT scanning was performed to obtain the location of individual microspheres as described previously by Marxen et al. (19 and Fig. 1*A*). The Batson's no. 17 is invisible in these scans since its X-ray and mass density is approximately that of tissue. After macerating the kidneys for 5 days in 30% potassium hydroxide, a second CT scan of the remaining vascular cast in air (Fig. 1, *B* and *C*) was acquired to obtain geometric information on the arterial vasculature.

CT scanning was performed using an MS90 eXplore Locus SP MicroCT scanner (General Electric Medical Systems, London, Ontario). The performance of this cone-beam CT scanner with rotating sample has been described in detail by Marxen et al. (20). For this

Address for reprint requests and other correspondence: R. M. Henkelman, Hospital for Sick Children Mouse Imaging Centre, 555 Univ. Ave, Toronto, Ontario, Canada M5G 1X8 (e-mail: mhenkel@phenogenomics.ca).

The costs of publication of this article were defrayed in part by the payment of page charges. The article must therefore be hereby marked "*advertisement*" in accordance with 18 U.S.C. Section 1734 solely to indicate this fact.

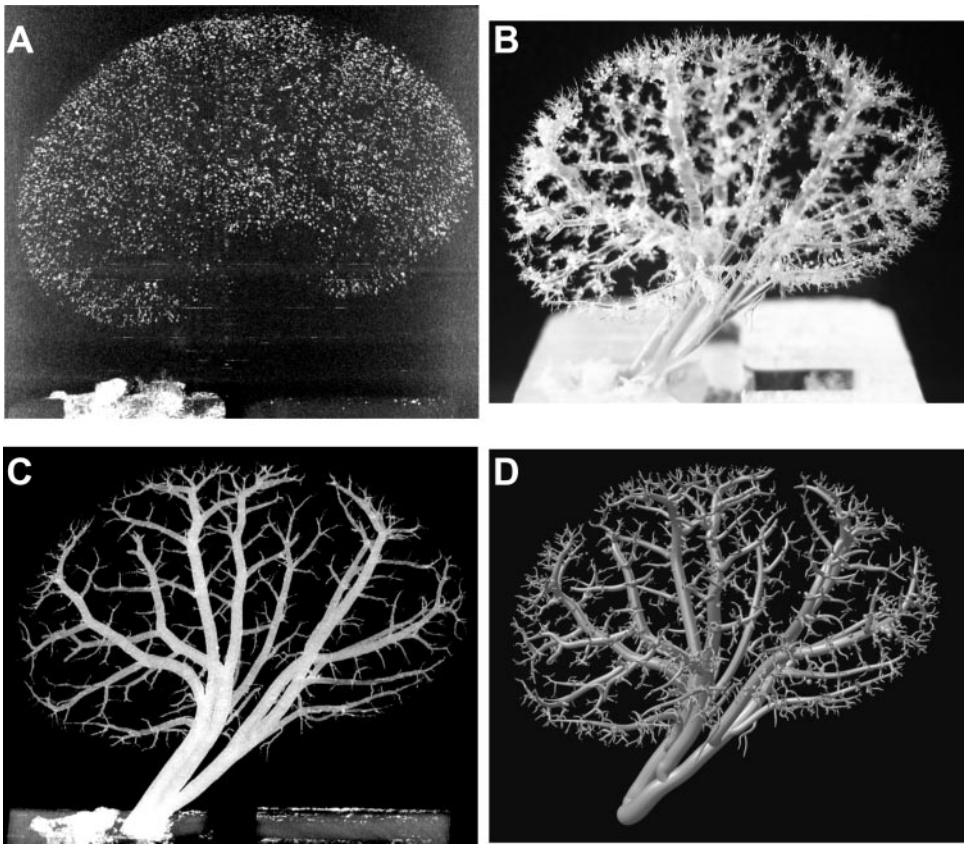

Fig. 1. *A*: maximum intensity projection (MIP) of microcomputed tomography (microCT) image of microspheres inside the left kidney. *B*: photograph of the arterial vascular cast after maceration of the tissue. *C*: MIP of the microCT image of the cast. *D*: rendering of the tubular model reconstructed from *C*. The geometry of the tubular structure is the basis of the flow model and registered with the particle image in *A* to obtain measurements of blood flow through each segment.

study, all scans were acquired with a detector pixel size in the object plane of 17 μm at 80 kV peak tube voltage and an exposure of 2,592 mA. Each scan took ~12 h. The size of the reconstructed volume elements (voxels) was 17 μm for the microsphere scans to optimize identification of the metal-coated microspheres and 34 μm for the cast scans to improve signal-to-noise ratio for automated reconstruction of the vascular tree. The resolution differences are immaterial to the analysis.

Cylindrical pipe model of the arterial tree. The method of extracting geometric information about the arterial tree from the cast scans has been described by Sled et al. (28). Briefly, CT images were thresholded, and a seeded growing region (1) was applied to separate vessels from background tissue. Based on the distance transform, which marks the closest distance of each voxel within a vessel to the vessel wall, the vascular tree was reduced to a skeleton of thin segments allowing the location of all branching points to be identified. A reconstructed cylindrical pipe representation of the arterial tree is shown in Fig. 1*D*. Vessel segments are defined as the connections between two subsequent branching points in the vascular tree. The segment radius is calculated as the average of the distance transform along the centerline of the vessel. The maximum error in the diameter measurements is approximately two voxels (20) or 70 μm. Segment length is defined as the distance from one branch point to the next along the centerline of the vessel.

It should be noted that this reconstruction of the vascular tree in the kidney is similar to that described by Kaimovitz et al. (15) for the heart. However, in the present case, the vascular tree is a faithful replica of the arteries in the particular kidney, and not just conforming to the average statistical properties.

Perfusion zones. Each voxel of the manually segmented kidney cortex parenchyma is assigned to a terminal segment of the arterial tree, the segment for which the distance of the voxel center to the end point of the segment divided by the terminal segment diameter is minimal. The diameter weighting in this nearest-neighbor approach accounts for the fact that larger terminal segments are expected to feed larger volumes. We refer to the sum of all voxels associated with a particular terminal segment as its fed volume. These fed volumes approximate the volume of tissue perfused by the associated terminal arteriole. Similarly, after the microsphere particle data are registered with the cast data, particles are also assigned to terminal segments. As one moves up the arterial tree from smaller to larger vessels, both fed volumes and particle numbers of the "left" and "right" daughter branches are added at each branching point resulting in fed volumes and particle numbers for all segments. Particle numbers are regarded as proportional to flow assuming complete mixing of microspheres and no recirculation. Particle number divided by the fed volume represents an approximation of the average perfusion in the volume fed by a particular segment. Note that fed volume is an approximation of the real perfusion volume of a particular segment. This approximation becomes increasingly realistic for larger segments because the accurate positions of the perfusion zone boundaries become less significant as fed volumes are aggregated.

Blood flow modeling. The details of the flow model have been described previously by Marxen (18) and are essentially the same as those described by Mittal et al. (21). Briefly, the resistance of each vessel segment is calculated based on Poiseuille's law. Given that the cast data do not include the smallest arterioles, an additional resistance depending on the terminal fed volume is assigned to each terminal segment assuming that segment conductance down to the level of the capillaries behaves like a power law as a function of fed volume. The power law parameters were estimated based on the measured data. Assuming a constant input pressure at the renal artery and a constant exit pressure at the capillary level, flow through each segment was calculated. Model perfusion was then calculated based on the same fed volumes as for the microsphere data.

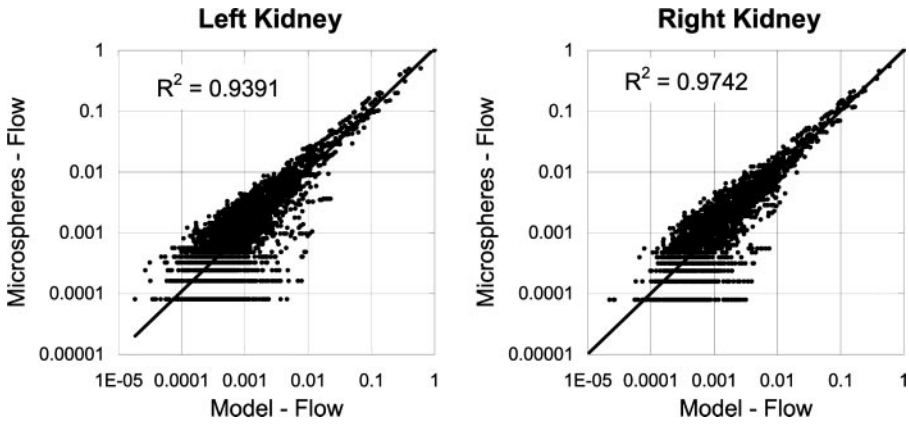

Fig. 2. Comparison of relative flow predictions based on the model with the microsphere data for vessel segments with one or more associated particles. The lowest horizontal line of data corresponds to vessel segments with only one associated particle. Pearson correlation coefficients on the log-log representations are quoted, and the line is the best fit to the data. Units are normalized to total flow at the renal artery.

Measuring perfusion heterogeneity. RD of perfusion within the kidney cortex is calculated as a function of scale V, with V being the average sample volume for a given partitioning of the specimen:

$$RD(V) = \sqrt{\frac{1}{P_{tot}^2}\sum_i \frac{V_i}{V_{tot}}(P_i - P_{tot})^2 - \frac{1}{\overline{X}}},$$

and V_i being the volume of an individual sample, V_{tot} being the total volume of the manually segmented kidney cortex, P_i being the perfusion within an individual sample volume, and P_{tot} being the average perfusion, which is independent of scale. $\overline{X}$ is the average number of particles found per sample volume. Thus $1/\overline{X}$ represents the square of the RD of the expected Poisson noise (6, 25). This correction is only applied for the microsphere data because it is irrelevant for the model calculations. Two different approaches were used to computationally dissect the cortex into individual sample volumes of different scales. The first approach is referred to as the "grid method" and resembles the standard methodology originally introduced by Bassingthwaighte et al. (2, 3). In this method, the tissue was physically cut into cubes and analyzed for microsphere content. As a computer analogy, a Cartesian square grid is overlaid on top of the cortex, and sample volumes are generated as the intersection of the individual grid volume elements with the cortex as described by Marxen et al. (19). The second approach ("fed volume method") partitions the specimen into regions of approximately size V associated with single vessel segments (i.e., branches of the tree) and that sum up to the total fed volume.

RESULTS

The number of microspheres found in the cortex of the left and right kidney were 12,438 and 12,752, respectively. This is a large number given that the rat kidney has ~36,000 glomeruli (10). The reason for using such a large number is that as the tissue is divided into smaller and smaller subvolumes, we still want enough microspheres for a precise estimate of perfusion. It has been suggested that 400 microspheres is an appropriate number (6). Once the volume of tissue contains only a few microspheres, the error on the calculated perfusion and the estimate of RD becomes meaningless. Clearly, the number of microspheres that we have used and the associated level of microvascular blockage will disrupt the subsequent physiological flow pattern. However, because this experiment is acute and the microspheres are all delivered in a single bolus, we believe that the deposition pattern is representative of the instantaneous steady-state flow. Figure 1*A* is a maximum intensity projection showing the particles in the left kidney. As shown in Fig. 2, flow model calculations and microsphere data are highly correlated with respect to blood flow. Figure 3 gives a visual impression of the distribution of local perfusion associated with each segment of the reconstructed arterial tree. The model trees consist of 4,203 segments in the case of the left kidney and 3,239 segments for the right kidney. A small systematic increase of microsphere-measured perfusion in the downward direction (7) is apparent in Fig. 3, which is not modeled in the calculations.

Figure 4 is a comparison of perfusion as predicted by the model with perfusion as measured using microspheres for the 500 segments with the largest particle numbers. These segments span a vessel diameter range from 1 mm to 120 μm (an 8-fold variation) and a fed volume range from 980 to 3 mm^3 (a 300-fold range). These volumes contain associated particle counts of ~12,500–100 (a 100-fold range). The mean perfusion (the total flow divided by the total fed volume) is normalized to one for both the experimental microsphere and calculated model results to allow for comparison. The SD of perfusion, which is a function of the scale of the included vessel segments, is two- to threefold larger for the microsphere data than for the model predictions. The fact that the measured perfusion is all between one-half and two times the mean (a 4-fold range) shows that different parts of the kidney (ranging in volume over 300-fold) are all perfused similarly but that the perfusion is not homogeneous. The calculated model perfusions are more tightly clustered about their mean with a range of less than twofold. However, no correlation between the flow model of deviation from homogeneous perfusion and the microsphere measurements of perfusion inhomogeneity is found. The broader dispersion in the microsphere direction than in the model calculation direction is believed to be real. When we extend this scatter plot to smaller vessels, this asymmetry persists. Eventually, the few microspheres in small volumes caused the scatter plot to get even more disperse in the microsphere direction. Consider the RD plots shown in Fig. 5 that summarize the variance in the scatter plot of Fig. 4 at differing sizes of the fed volume. Figure 5 also accounts for the additional variance coming from the Poisson statistics of a few microspheres.

Figure 5 is a comparison of RD curves of the modeled and measured perfusion data. The measured RD values are about two- to threefold higher than the modeled data, which is consistent with Fig. 4. To generate these curves, the mass of tissue used in the denominator was the associated fed volume. Alternatively, the tissue volume can be "cut up" using a

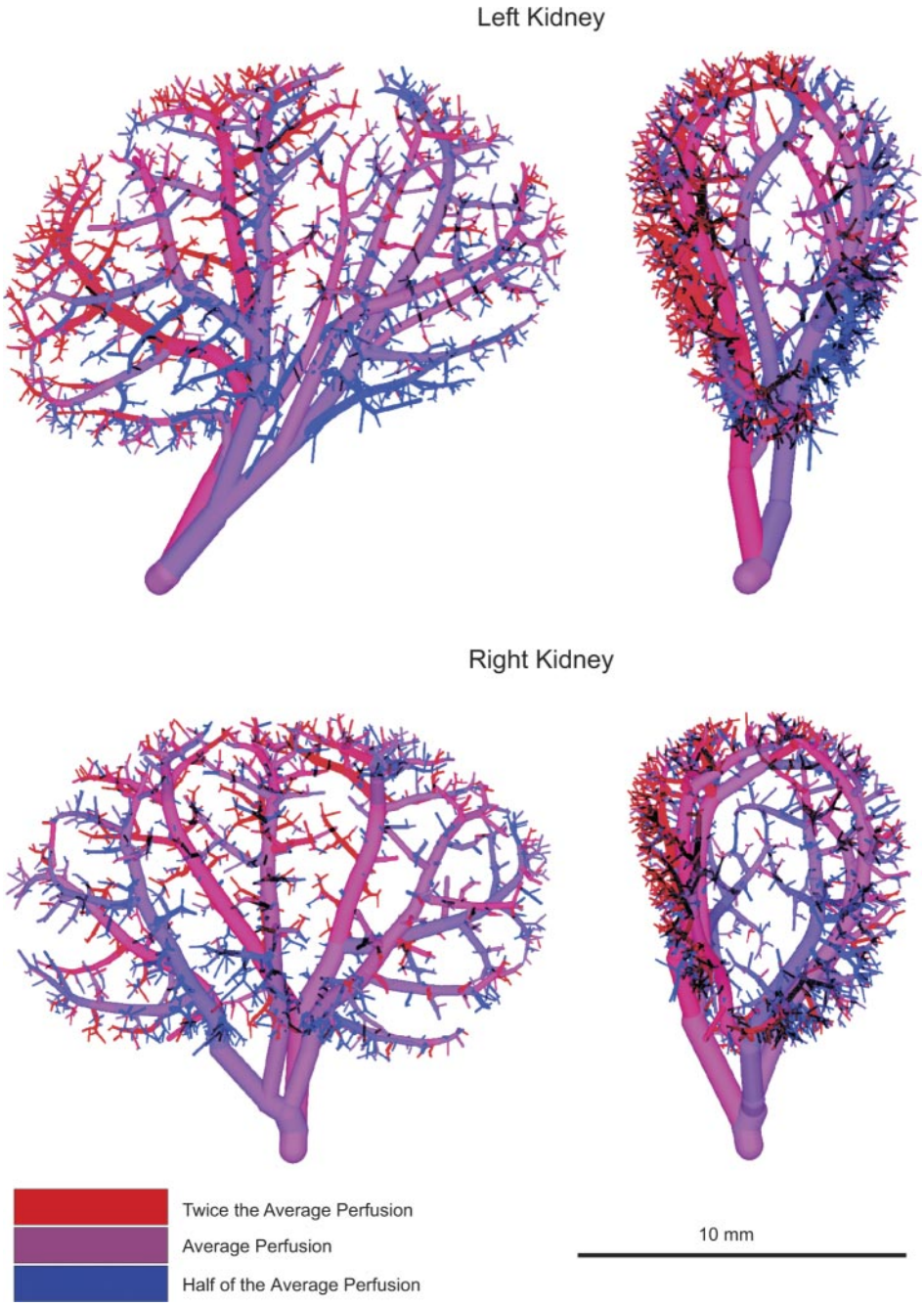

Fig. 3. Color-coded image of perfusion associated with each vessel segment based on microsphere data. Each kidney is shown in two views [anterior/posterior (A/P) on *left* and superior/inferior (S/I) on *right*]. With the rat in the supine position during microsphere injection, the posterior direction (downward) is into the page for the (A/P) views and toward the left in the (S/I) views.

rectilinear grid as is typically done for experimental measures of RD. The RD curves of the microsphere data that were generated with the standard grid method closely follow a linear relationship on a double-logarithmic plot. This behavior confirms the fractal behavior of the RD data generated by the grid method (3). The slopes of these grid curves (approximately −0.2) are similar to published measurements in the heart (2) and lungs (11). Segmentation using the fed volume sampling method shows a similar linear relationship on a double-logarithmic plot but with a more negative slope (−0.25 to −0.31). RD is very similar for both the grid and fed volume methods for small sample volumes, but the grid sample method produces higher dispersion for large sample volumes. Dissecting the tissue along physiologically more meaningful fed volume boundaries gives, therefore, a more homogeneous picture of perfusion at large scales. The linear regression lines for the calculated flow model give an even steeper slope (−0.35 to −0.40) of the RD compared with the measured curves.

DISCUSSION

The observed high correlation with respect to flow between the model and the microsphere measurements indicates that both the model and the measurements represent, in a first approximation, a consistent picture of blood flow. Both the model flow calculations and the microsphere measurements of perfusion show that perfusion of this organ is approximately constant to within a factor of 2–4 even though the sampled

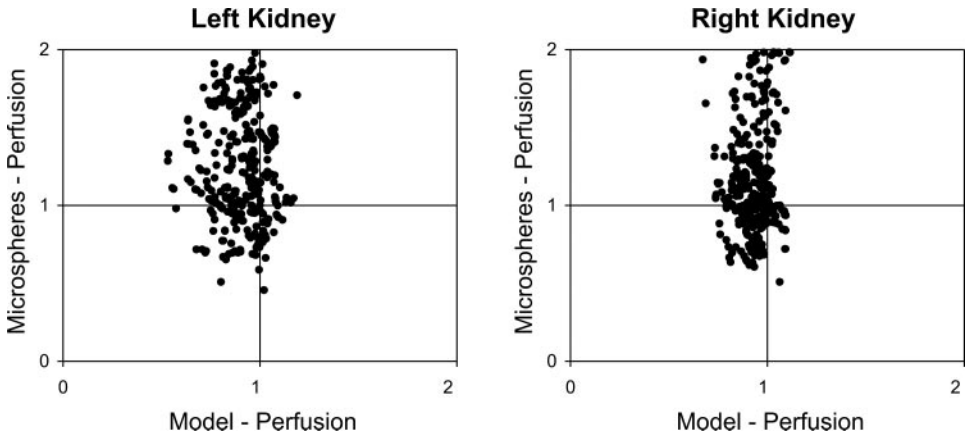

Fig. 4. Comparison of normalized perfusion as measured by the microsphere technique with the calculated flow model values for the 500 segments with the largest numbers of associated microspheres.

volumes range over a factor of 300. That the residual deviations from homogeneous perfusion are not correlated between calculation and experiment might be expected given the limited accuracy of both the measurements and the model. The measurements are corrected for Poisson noise, which is a small effect in the larges volumes but contributes much of the variance in the smallest segments where the particle count goes down to 100 ± 10. The flow calculations, on the other hand, are continuous and thus do not have this source of stochastic noise. Also, the influence of gravity on the metal-coated microspheres (density = ~2 g/ml compared with conventional microspheres ~1.3 g/ml) may influence the experimental results, although this is denied by published results over the range of 1–3 g/ml (26, 27). No such density variation affects the flow calculations. Also, there have been reports of skimming (disproportionate segregation of microspheres at asymmetric branchings in the vasculature; see Ref. 23). Again, there is no equivalent effect in the flow. There has also been evidence that skimming of microspheres causes disparate branch flows at asymmetric branchings (23).

The slopes of the RD curves for the microsphere data generated using the grid methodology (approximately −0.2) are similar to slopes quoted by Grant and Lumsden (13) for contrast-enhanced CT images of cortical perfusion as well as to slope data from the heart (2) and lungs (11). It should be noted that the logarithmic data generated by the grid methodology are well represented by a linear slope model, which indicates that the RD is fractal (3). However, the differences in slope between the grid and volume methods indicate a dependence on the process used to subdivide the tissue. The slope of the RD curve contains information about the correlation of perfusion in neighboring sample volumes. A slope of −0.5 would be expected for uncorrelated data, whereas slopes between 0 and −0.5 indicate a positive correlation (3). The more homogeneous data generated by the flow model appear to be less correlated. However, the logarithmic data for the fed volume RD curve of the left kidney and for both flow model curves are not satisfactorily represented by a straight line, which makes the value of a detailed comparison of slopes of limited value.

In conclusion, this study shows that specific model-based calculations of flow correlate well with microsphere measurements and that both correspond to relatively homogeneous perfusion in the kidney. This presented approach compares for the first time models of flow through reconstructed arterial trees and measurements of flow within a single organ. This new combined approach will improve our understanding of the relationship between arterial geometry and the local distribution of perfusion. The methodology is more powerful than simple analysis of RD curves because it is based on knowledge of both vascular structure and the locations of individual perfused microspheres, and may therefore aid in the interpretation of RD data.

The lack of correlation found between the computational model of perfusion heterogeneity and the microsphere measurements of perfusion heterogeneity at equivalent locations is not yet understood. It may simply result from imprecision in both the computational fluid dynamic model and the microsphere measurements. Alternatively, it may signal a lack of

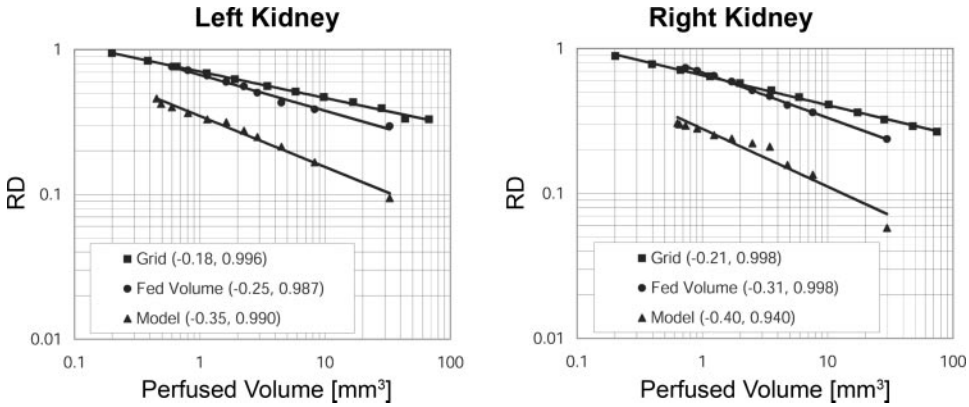

Fig. 5. Comparison of predicted and measured relative dispersion (RD) curves. Analyses were conducted using the grid method and the fed volume method as described in the text. Slopes of the regression lines for the logarithmic data and R^2 values are given in parentheses. A slope of −0.5 would indicate a random spatial distribution.

fidelity between blood flow and microsphere delivery as suggested by Decking et al. (9). This could arise from "channeling" of microspheres along dominant arteriole branches, inadequate mixing, gravity effects on microsphere filling, inadequate detail in the flow model from ignoring pulsatile flow and vessel elasticity, or a host of other possibilities. To quote from Decking et al. (9), "Clearly, future studies are needed relating local flow to local microspheres deposition at the intermediate scales." The technique we have described in this paper provides a useful method for these future studies.

GRANTS

This research was supported by the Canadian Institutes of Health Research and the National Cancer Institute of Canada. R. M. Henkelman is the recipient of a Canada Research Chair in Imaging.

REFERENCES

1. **Adams R and Bischof L.** Seeded region growing. *IEEE Trans Pat Anal Machine Intel* 16: 641–647, 1994.
2. **Bassingthwaighte JB, King RB, and Roger SA.** Fractal nature of regional myocardial blood flow heterogeneity. *Circ Res* 65: 578–590, 1989.
3. **Bassingthwaighte JB, Liebovitch LS, and West BJ.** *Fractal Physiology*. Oxford, UK: Oxford Univ, 1994.
4. **Bauer WR, Hiller KH, Galuppo P, Neubauer S, Kopke J, Haase A, Waller C, and Ertl G.** Fast high-resolution magnetic resonance imaging demonstrates fractality of myocardial perfusion in microscopic dimensions. *Circ Res* 88: 340–346, 2001.
5. **Beard DA and Bassingthwaighte JB.** The fractal nature of myocardial blood flow emerges from a whole-organ model of arterial network. *J Vasc Res* 37: 282–296, 2000.
6. **Buckberg GD, Luck JC, Payner DB, Hoffman JIE, Archie JP, and Fixler DE.** Some sources of error in measuring regional blood flow with radioactive microspheres. *J Appl Physiol* 31: 598–604, 1971.
7. **Clough AV, Haworth ST, Friedman J, Dawson CA, and Hoffman EA.** Radiopaque contrast medium distribution: influence of gravity on X-ray flow measurements. *Biomedical Engineering Society Annual Meeting Seattle, WA,* 2000.
8. **Crawford MW, Leman J, Saldivia V, and Carmichael FJ.** Hemodynamic and organ blood flow responses to halothane and sevoflurane anesthesia during spontaneous ventilation. *Anesth Analg* 75: 1000–1006, 1992.
9. **Decking UKM, Pai VM, Bennett E, Taylor JL, Fingas CD, Zanger K, Wen H, and Bassingthwaighte JB.** High-resolution imaging reveals a limit in spatial resolution of blood flow measurements by microspheres. *Am J Physiol Heart Circ Physiol* 287: H1132–H1140, 2004.
10. **Fortepiani LA, Ortiz Ruis MC, Passardi F, Bentley MD, Garcia-Estan J, Ritman EL, and Romero JC.** Effect of losartan on renal microvasculature during chronic inhibition of nitric oxide visualized by micro-CT. *Am J Physiol Renal Physiol* 285: F852–F860, 2003.
11. **Glenny RW, Bernard SL, and Oberson HT.** Pulmonary blood flow remains fractal down to the level of gas exchange. *J Appl Physiol* 89: 742–748, 2000.
12. **Glenny RW and Robertson HT.** A computer simulation of pulmonary perfusion in three dimensions. *J Appl Physiol* 79: 357–369, 1995.
13. **Grant PE and Lumsden CJ.** Fractal analysis of renal cortical perfusion. *Invest Radiol* 29: 16–23, 1994.
14. **Iversen PO and Nicolaysen G.** Fractals describe blood flow heterogeneity within skeletal muscle and within myocardium. *Am J Physiol Heart Circ Physiol* 268: H112–H116, 1995.
15. **Kaimovitz B, Lanir Y, and Kassab GS.** Large-scale 3-D geometric reconstruction of the porcine coronary arterial vasculature based on detailed anatomical data. *Ann Biomed Engineer* 33: 1517–1535, 2005.
16. **Kalliokoski KK, Kuusela TA, Nuutila P, Taolvanen T, Oikonen V, Teras M, Takala TE, and Knuuti J.** Perfusion heterogeneity in human skeletal muscle: fractal analysis of PET data. *Eur J Nucl Med* 28: 450–456, 2001.
17. **Karch R, Neumann F, Podesser BK, Neumann M, Szawlowski P, and Schreiner W.** Fractal properties of perfusion heterogeneity in optimized arterial trees: a model study. *J Gen Physiol* 122: 307–321, 2003.
18. **Marxen M.** *Fractal Characteristics of Vascular Structure and Modeling of Blood Flow in Three Dimensions* (PhD dissertation). Toronto, Ontario: University of Toronto, 2005.
19. **Marxen M, Paget C, Yu LX, and Henkelman RM.** Estimating perfusion using microCT to locate microspheres. *Phys Med Biol* 51: N9–N16, 2006.
20. **Marxen M, Thornton MM, Chiarot CB, Klement G, Koprivnikar J, Sled JG, and Henkelman RM.** Micro CT scanner performance and considerations for vascular specimen imaging. *Med Phys* 31: 305–313, 2004.
21. **Mittal N, Zhou Y, Linares C, Ung S, Kaimovitz B, Molloi S, and Kassab GS.** Analysis of blood flow in the entire coronary arterial tree. *Am J Physiol Heart Circ Physiol* 289: H439–H446, 2005.
22. **Nagao M, Sugawara Y, Ikeda M, Fukuhara R, Holoiski K, Murasa K, Mochizuki T, Miki H, and Kikuchi T.** Heterogeneity of cerebral blood flow in frontotemporal lobar degeneration and Alzheimer's disease. *Eur J Nucl Med Mol Imaging* 31: 162–168, 2003.
23. **Ofjord ES, Clausen G, and Aukland K.** Skimming of microspheres in vitro: implications for measurement of intrarenal blood flow. *Am J Physiol Heart Circ Physiol* 241: H342–H347, 1981.
24. **Parker JC, Cave CB, Ardell JL, Hamm CR, and Williams SG.** Vascular tree structure affects lung blood flow heterogeneity simulated in three dimensions. *J Appl Physiol* 83: 1370–1382, 1997.
25. **Polissar NL, Stanford DC, and Glenny RW.** The 400 microsphere per piece "rule" does not apply to all blood flow studies. *Am J Physiol Heart Circ Physiol* 278: H16–H25, 2000.
26. **Prizen FW and Bassingthwaighte JB.** Blood flow distributions by microsphere deposition methods. *Cardiovasc Res* 45: 13–21, 2000.
27. **Reed JH Jr and Wood EH.** Effect of body position on vertical distribution of pulmonary blood flow. *J Appl Physiol* 28: 303–311, 1997.
28. **Sled JG, Marxen M, and Henkelman RM.** Analysis of micro-vasculature in whole kidney specimens using micro-CT. *Proceedings of the SPIE 49th Ann Meet Int Symposium Optical Sci Technol, 2004*.
29. **VanBavel E and Spaan JA.** Branching patterns in the porcine coronary arterial tree. *Circ Res* 71: 1200–1212, 1996.
30. **van Beek JH and Roger SA.** Regional myocardial flow heterogeneity explained with fractal networks. *Am J Physiol Heart Circ Physiol* 257: H1670–H1680, 1989.